UNIVERSITY OF OKLAHOMA

GRADUATE COLLEGE

BIG-DATA ANALYTICS OF HUMAN BRAIN NETWORK DYNAMICS:

A SIMULTANEOUS EEG-FMRI STUDY

A THESIS

SUBMITTED TO THE GRADUATE FACULTY

in partial fulfillment of the requirements for the

Degree of

MASTER OF SCIENCE

By

JULIA TANG
Norman, Oklahoma
2020

BIG-DATA ANALYTICS OF HUMAN BRAIN NETWORK DYNAMICS:
A SIMULTANEOUS EEG-FMRI STUDY

A THESIS APPROVED FOR THE
STEPHENSON SCHOOL OF BIOMEDICAL ENGINEERING

BY THE COMMITTEE CONSISTING OF

Dr. Han Yuan, Chair

Dr. Lei Ding

Dr. Jerzy Bodurka

Acknowledgments

I would like to extend my profound gratitude to my advisor, Dr. Han Yuan. It is my honor to be her student. She never gives up on me, no matter the circumstances. On many occasions, Dr. Yuan has made herself available late nights to discuss my research questions and save me in the nick of time in revisions. She has taught me the essentials of coding without taking advanced computer science classes, and deepened my understanding, cultivating my passion in the computational field of biomedical engineering. As an instructor, she diligently taught my classes with enthusiasm and technique, making her classes engaging and applicable to all areas of my research. Her mentorship in both research and my career have been invaluable.

I would like to thank my committee members, Dr. Lei Ding and Dr. Jerzy Bodurka, for their support and teachings throughout my engineering career. Both of these remarkable instructors developed my understanding of bioinstrumentation through their teaching, and I would not have been able to complete my work without their instruction.

Lastly, I would like to thank the grants that supported me, my research, and this ongoing project for making all of this possible. This work was supported by NIH/NIGMS P20 GM121312, and NSF RII Track-2 #1539068, and Institute for Biomedical Engineering, Science and Technology at the University of Oklahoma.

Table of Contents

List of Tables

List of Figures

Abstract

Psychiatric conditions, such as mood and anxiety, are complex and heterogeneous syndromes that encompass varied, co-occurring symptoms and divergent responses to treatment. To facilitate characterizing the heterogeneity of neuropsychiatric disorders, we used a multimodal functional imaging approach to examine human brain connectivity. Here, we investigated data from the Tulsa-1000 study, including electroencephalographic (EEG) recordings, functional magnetic resonance imaging (fMRI) and structural MRI data, behavior tests, and psychological and clinical assessments acquired from 288 subjects. The electrical brain activity was analyzed using the temporal independent EEG microstates (EEG-ms), a technique that can measure dynamic neural activity. Using a data-driven approach, we examined the properties of EEG-ms in both Mood and Anxiety (MA) patients and healthy controls (HC) subjects. We found distinctive EEG-ms associated with the dorsal default mode network and anterior salience network in both MA group and healthy controls. Specifically, the occurrence rate of the dorsal default mode network was positively correlated with rumination response in the MA group. Our results reveal a novel finding of abnormal neural dynamics and contribute to the underlying pathophysiological mechanisms of MA. Implications of this technology can provide new insights into understanding the biological mechanism of mood and anxiety disorders.

Chapter 1: Introduction and background

Psychiatric conditions, such as mood and anxiety (MA), are complex and heterogeneous syndromes that encompass varied, co-occurring symptoms and divergent responses to treatment. For example, neuropsychological investigations have revealed that in depressive disorders, there is an increased tendency to recall adverse events (Watkins et al., 1996), blunted response to positive stimuli (Young et al., 2014), and exaggerated response towards negative feedback (Elliott et al., 1997). On the other hand, anxiety disorder is characterized by chronic worrying, ruminative thinking, and stereotyped actions aimed at relieving anxious thoughts amongst others (Paulus & Stein, 2010). Because these disorders are often comorbid, they are often difficult to diagnose and treat. Thus, the need for proper detection and characterization of these disorders is critical. In addition to current symptom-focused classification, we can look into the underlying mechanisms of the psychiatric disorder by using brain imaging tools to investigate functional networks. Functional networks are the collection of specific brain regions with activity that tends to increase or decrease simultaneously when at rest or while performing cognitive tasks. By using brain imaging approaches, abnormalities can be objectively identified with greater efficiency and accuracy, resulting in better, more tailored treatment approaches (Sylvester et al., 2012).

In this study, we specifically focused on mood and anxiety disorders because they involve alterations in emotion regulation networks and brain regions such as default mode, salience networks, cingulate cortex, hippocampus, and amygdala (Sylvester et al., 2012). Notably, the default mode network (DMN) and the salience network (SN) are functional

networks that affect our memory and regulate the likelihood that an event will be remembered and recalled.

To further our understanding of the underlying mechanisms of these aberrant cognitive and emotion processing in psychiatric disorders, we can assess the temporal dynamics of brain activity. This can be elucidated by EEG microstates. EEG microstates, or EEG-ms, are distinct topographic representations of EEG, lasting a few milliseconds. The functional interpretation of EEG-ms can be explained as coordinated and synchronized neuronal current activity of many neurons from different regions of the brain that activate simultaneously. Changes in topographies of these EEG-ms can be attributed to the change in orientation or current dipoles. Yuan et al. (2012) reported that spatially independent EEG-ms and especially, temporally independent EEG-ms were shown to be correlated with blood-oxygenation-level-dependent (BOLD) resting-state networks (RSNs) as revealed by functional magnetic resonance imaging (fMRI). Their study and others (Brandeis et al., 1995; Brandeis & Lehmann, 1989) demonstrated that EEG-ms can characterize network changes and disruptions in brain functionality from psychological disorders and can become valuable potential biomarkers.

The primary goal of this study is to further explore the possible association among the EEG-ms dynamic patterns during resting state, especially in those with mood and anxiety disorders. Multimodal functional imaging—specifically simultaneous fMRI and EEG—of the human brain provides a unique capacity to research and characterize the heterogeneity of neuropsychiatric disorder because it combines the high spatial resolution of the fMRI and the high temporal resolution of EEG to improve the caliber of measurement from either instrument alone. Here, we established automatic big-data analytics to remove MR-related noises in EEG and performed multimodal analysis using the method described in Wong et al. (2016, 2018) and

Yuan et al. (2012). We hypothesize that (1) there should be significant differences in EEG-ms-informed RSNs in default-mode and salience network between mood anxiety (MA) and healthy control (HC) group, and (2) EEG-ms temporal dynamics will be associated with the psychological symptoms measured from clinical examinations. These correlations will be useful for translational purposes.

Chapter 2: Methodology

2.1: Demographics

Participants were selected from the Tulsa-1000 (T1000) study (Victor et al., 2018), which compiled simultaneous EEG and fMRI data, behavior tests, psychological and clinical assessments, and structural MRI from a large dataset of 1000 subjects in total. The T-1000 naturalistic study was conducted at the Laureate Institute of Brain Research in Tulsa, Oklahoma**.** The T-1000 study investigated how mood and anxiety disorders, substance use, and eating behavior, organized across different levels of analysis, could predict long term prognosis, symptom severity and treatment outcome. Participants who underwent and completed all phases of the study were considered for analysis (n = 500). Of these participants, 56 were healthy controls (HC), 232 were mood anxiety (MA) patients, 159 had substance abuse, and 19 had eating disorders. Only MA and HC were used for further analysis. Those who had MA, were clinically diagnosed with either depression (n = 65), anxiety disorder (n = 18), or both (n = 149). Those with eating disorders and/or substance abuse were excluded. Screening, as described in Victor et al (2018), was based on their psychopathological scores i.e. Patient Health Questionnaire-9 (PHQ-9) and Overall Anxiety Severity and Impairment Scale (OASIS) and treatment-seeking history. See Table 1 for more details.

All protocols were approved by Western Institutional Review board. All participants signed the informed consent form. All subjects received financial compensation for their participation.

Table 1: Demographic characteristics

CHARACTERISTIC	*HC (N = 56)*	*MA (N=232)*
Age (mean ± SD years)	32.3 ± 11.0	36.3 ± 11.1
Female/Male	29 / 27	176 / 71
PHQ-9 (mean ± SD)	1.39 ± 0.91	12.7 ± 5.1
PROMIS Anxiety (mean ± SD) ***	46.5 ± 7.9	62.9 ± 6.7
PROMIS Depression (mean ± SD) ***	44.4 ± 7.9	61.1 ± 7.6
RRS score (mean ± SD) ***	30.1 ± 8.0	55.3 ± 11.9
RRS Reflection sub-score (mean ± SD) ***	7.16 ± 2.8	11.2 ± 3.3
RRS Depression sub-score (mean ± SD) ***	14.3 ± 4.8	31.3 ± 7.4
STAI Trait (mean ± SD) **	28.6 ± 7.3	53.8 ± 10.6
TAS-20 (mean ± SD) ***	49.2 ± 8.3	59.0 ± 9.9

HC: Healthy Controls; MA: Mood and Anxiety; PHQ: Patient Health Questionnaire-9; PROMIS: Patient-Reported Outcomes Measurement Information System; RRS: Ruminating Response Score; STAI: State Trait Anxiety Inventory; TAS-20: Toronto Alexithymia Scale; SD: standard derivation; ***represents ($p<0.001$), **represents nonparametric test was used ($p<0.001$).

The primary diagnostic clinical scores were the PHQ-9 and Patient-Reported Outcomes Measurement Information System (PROMIS) Anxiety and Depression. All participants reported characteristic and psychological scores such as the STAI, TAS-20, and RRS. Two sub-scores from RRS, reflection and depression, were calculated post-hoc (Treynor et al., 2003).

2.2: Data Acquisition

Simultaneous EEG-fMRI measurements at eyes-open resting state were acquired. Participants were instructed to fixate their gaze on a cross displayed on the fMRI stimulus projection screen. EEG data were recorded using an MR-compatible Brain Products (Brain Products GmbH, Germany) amplifier and 31-electrode cap, on a 3-Tesla MR750 MRI scanner (GE Healthcare, Milwaukee, WI). Resting fMRI data were acquired with EPI sequence (TR/TE = 2000/27ms, FOV/slice = 240/2.9mm, 39 axial slices), and each scan lasted 8 minutes. Respiration volume and cardiac pulse were also recorded. In this study, we analyzed simultaneously collected EEG and fMRI data and self-report questionnaire scores.

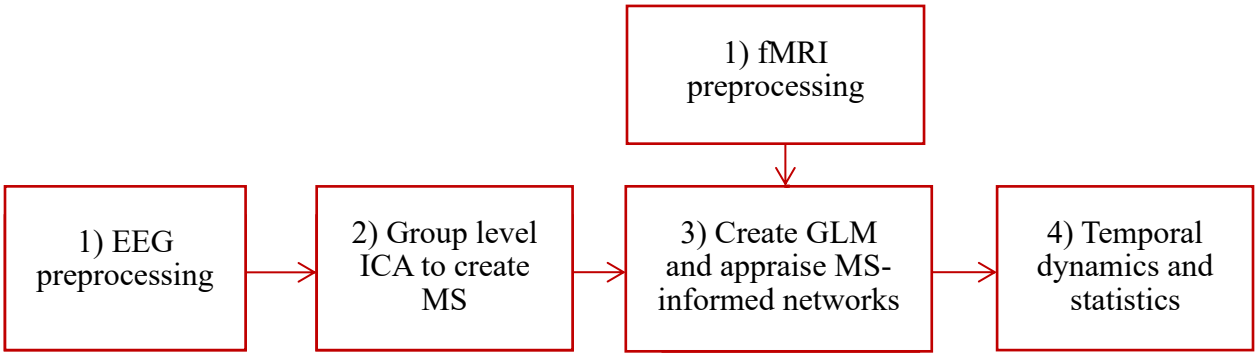

Figure 1: Simultaneous EEG-fMRI analysis flow chart.

From preprocessing to analysis of microstate temporal dynamics, the analysis of simultaneous EEG-fMRI data is shown in this diagram.

2.3 fMRI preprocessing

Resting-state fMRI preprocessing was done using Analysis of Functional NeuroImages software. (AFNI, http://afni.nimh.nih.gov/) (Cox, 1996). The first five volumes were removed to

ensure steady state was reached. Cardiac and respiration frequencies were removed through RETROICOR methods (Glover et al., 2000). Then the fMRI data were corrected for slice timing, aligned to anatomical images, censored out motion artifacts with a threshold of 0.25 mm, spatially transformed into stereotaxic Talairach array and smoothed.

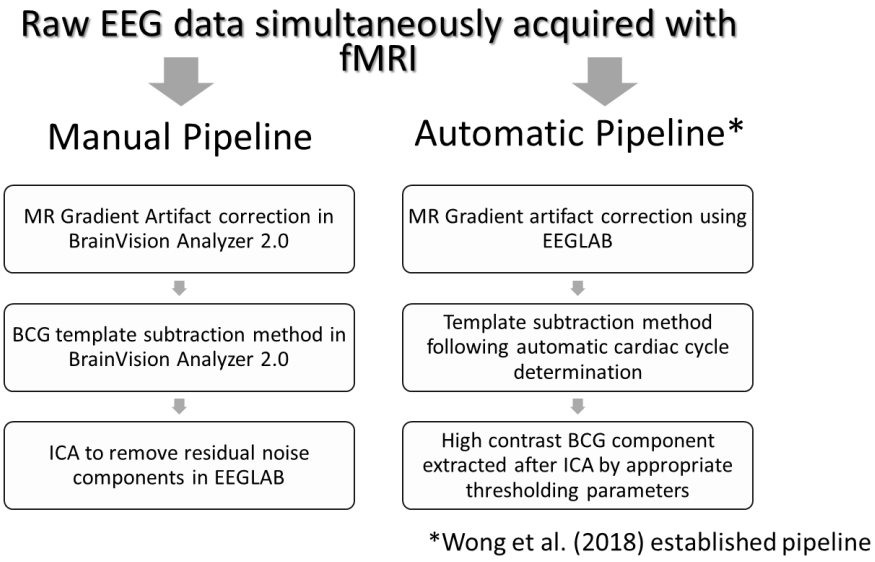

Figure 2: EEG Preprocessing flowchart.

Diagram of preprocessing steps for EEG data simultaneously acquired with fMRI using two pipeline methods.

2.3: Manual EEG preprocessing

In the preprocessing of EEG data, we adopted an automatic pipeline to remove the MR-related artifacts in the large dataset of my study. In addition, I have also performed manual preprocessing in a randomly selected subset of 20 subjects. I further assessed the quality of automatic preprocessing by comparing the outcomes of the 20 manually processed data to those of the same 20 subjects processed by the automatic pipeline.

Preliminary manual preprocessing was performed in BrainVision Analyzer 2.0 software, which included the reduction of MRI imaging artifacts and removal of cardiobalistic artifacts (BCG). We reduced the MR artifacts by utilizing the average artifact subtraction method (Allen et al., 2000), and EEG signals were downsampled to 250Hz. The average artifact subtraction method was also used for identifying and subtracting cardiac artifacts (Allen et al., 1998). Mechanical vibration noise at 26 Hz was filtered out.

Afterwards, the EEG data were exported into EEGLAB, where the data were bandpass filtered between 0.5 to 70Hz and notch filtered at 60Hz to remove AC power line noise. Common average re-referencing was applied to further minimize uncorrelated sources of noise. Independent component analysis (ICA) was then used to decompose the EEG signals. Manual inspection of EEG topographies and power spectrum density (PSD) plots were conducted to remove artifactual ICs (e.g. residual BCG and imaging, eye and muscle movement artifacts, and bad channels). EEG signals were then reconstructed with inverse ICA to back project the remaining ICs that were related to neural activities.

2.4: Automatic EEG preprocessing

We adapted an automatic preprocessing pipeline by Wong et al. (2010) which incorporated correction of MR gradient artifacts and ballistic cardiogram artifacts using independent component analysis methods. EEG signals were downsampled to 250Hz, bandpass filtered from 0.1 to 70Hz, and band-stop filter with 1Hz bandwidth at 26Hz and 60Hz. To ensure quality results, we compared the results of the pipeline with the manual standard of preprocessing until the differences were acceptable by the significance of spatial and temporal correlations (see Figure 1 for detailed preprocessing steps). After acceptable differences, we

continued with the pipeline to expedite preprocessing for the large dataset. With the pipeline, 118,500 data points were retained per session. No bad segments were removed for motion artifact correction. Three TRs, or six seconds, were removed from the start of each recording. The data were band-pass filtered from 1 to 70Hz and downsampled to 250Hz, and common average re-referenced.

2.5: Microstate analysis of EEG

After preprocessing, temporal independent EEG microstates (EEG-MS) were derived using the method described in Yuan et al. 2012. Two more TRs were later removed from the EEG data to align with fMRI preprocessing. Data from each subject were concatenated for group level analysis. To calculate the temporal dynamics of the data, the global field potential was found to maximize the signal to noise ratio of the clean data concatenated. Then the concatenated data ran through ICA to separate the components that made up the data. Uniquely, with ICA, each component was temporally independent. With a 31-channel EEG cap, the highest possible number of independent components (IC) that became a different microstate was 30. Back-projection allowed us to obtain maps associated with each microstate. Each IC corresponds to a spatial topology of a microstate and the intensity of the microstate can be seen in the temporal trace. At each timepoint, one microstate would be exclusively labeled based on the maximal absolute intensity value. This gave us a binary matrix where each "1" were assigned to microstate with the greatest absolute intensity value. Then to align the EEG data with the fMRI data, the normalized time courses were convolved with a double-gamma hemodynamic response function and downsampled to 0.5 Hz.

2.6: Combined fMRI analysis with EEG-ms

Networks that are associated with EEG-MS were matched to the fMRI resting state networks via a temporal and spatial double association approach (Yuan et al., 2012, 2018). In the temporal domain, the time courses of the BOLD RSNs to the temporal independent microstates (See Figure 3 for single subject comparison) were correlated. Then, we further examined the extent to which each microstate related spatially to the group level BOLD RSNs. This was performed by using a general linear model (GLM) to map the correlations from the regressor, the EEG-ms time course, to the local BOLD signal across the entire brain. The resulting map (Figure 9) revealed areas of the brain that are significantly correlated with the relevant EEG-ms time course. These MS-informed statistical maps were also compared to the spatial patterns from template networks created by Shirer et al. 2012.

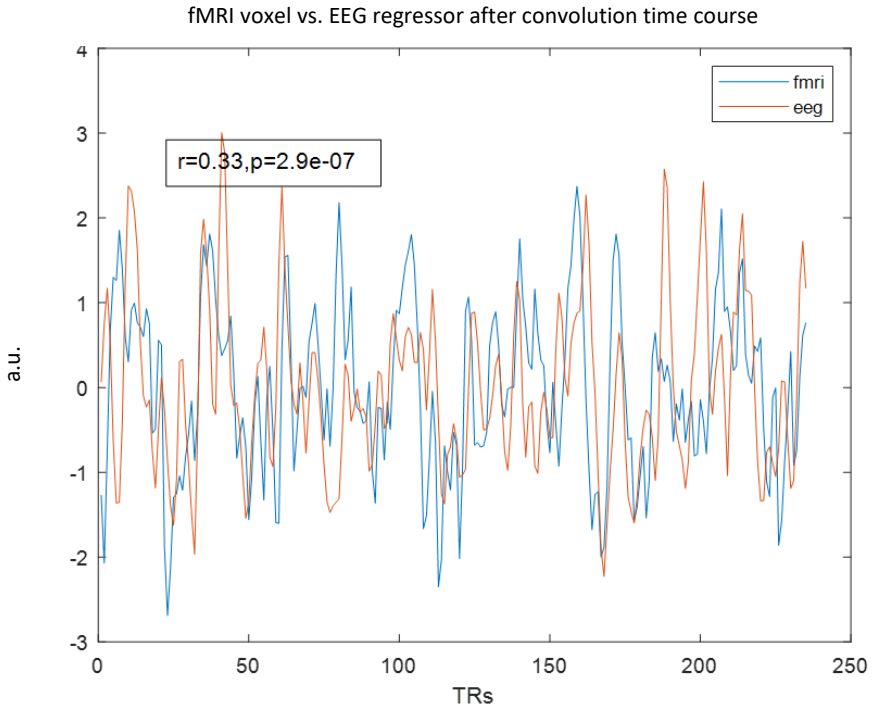

Figure 3: EEG and fMRI time courses related to dDMN in a single subject.

The z-scored fMRI time course (in blue) correlated with z-scored EEG-ms time course (in orange) after convolution with HRF in a single subject in MA cohort. EEG time course was derived by convolving the traces of MA IC9 and a hemodynamic response function. The fMRI time course was exacted and averaged from a region in the medial prefrontal region as part of the dorsal default mode network. The x-axis is the time domain on the scale of two seconds. Pearson's correlation was used to examine significance.

The significance criterion for detecting activation in the EEG-informed GLM analysis was set at $p_{corrected} < 0.05$ determined using the AFNI program 3dClustSim (cluster size > 90 voxels, thresholded at voxel uncorrected $p < 0.005$). The template networks were derived from Functional Imaging in Neuropsychiatric Disorders (FIND) Lab at Stanford University (Shirer et al., 2012), and the dice coefficient was calculated for the thresholded MS-informed fMRI network with uncorrected $p < 0.005$. Dynamic resting state functional connectivity was quantified as the occurrence frequency and duration of EEG-ms.

2.7: Statistical analysis

The significance of the dice coefficient found between the thresholded (using t statistic, calculated by T-test of means against 0's) MS-informed fMRI topographical map and the Stanford template was determined by a permutation test. It is important to note that the Stanford template was based on healthy brain activations. With over 239,000 voxels per mask, a random permutation of over 20,000 to scramble the mask of the template was performed to test for significant correlations between the two binary masks. A significant dice coefficient was indicative of how reliable our network map was compared to template.

2.7.1: T-test on temporal dynamics (MA vs. HC)

Once a meaningful and significant dice coefficient was acquired, temporal dynamics of the functional network of interest would undergo temporal analysis. All temporal dynamics, defined here by the occurrence ratings, were normally distributed. All matched significance was determined by $\alpha < 0.05$. Mean microstate duration was determined by the average time a single microstate dominated, largest global field power at a given time point, the recording. Median duration was also calculated, and typically lasted 20-30 ms. The frequency of each microstate was calculated as the total number of instances a microstate dominated the entire length of the recording divided by the total time. The occurrence percentage was taken as the total number of times one microstate dominated the recording divided by the total possible number of times.

2.7.2: Correlation of temporal dynamics vs. clinical scores

Finally, to find relevance with clinical symptoms, Pearson correlation was used to measure the strength of correlation compared between the temporal dynamics and to the respective cohort's clinical scores. The Bonferroni-Holm method, a sequentially rejective method compared to the simple Bonferroni method was used to strongly control for family-wise error rate at the alpha level, was used to account for multiple comparisons with a significance value of $p < 0.05$.

Chapter 3: Results

3.1: Quality check between automatic pipeline and manual pipeline

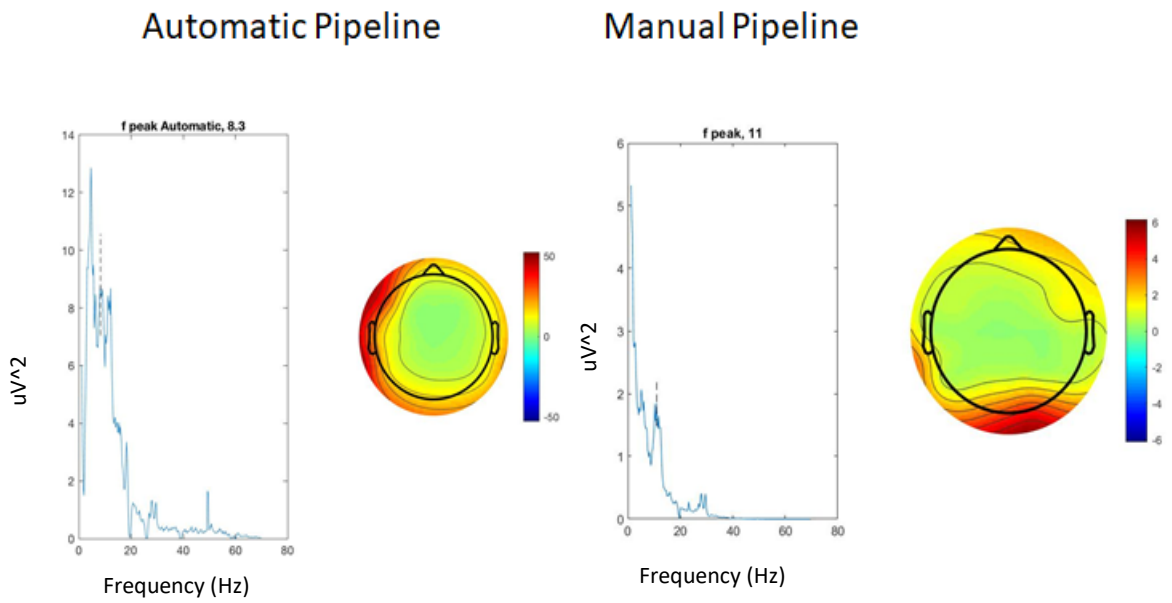

Figure 4: Single-subject EEG processed by automatic (Left) and manual (Right) pipelines. The spectrum was calculated from the signal at POz electrode and the topography shows the amplitude of EEG at the peak in the alpha band, illustrated by a dashed line on the spectrum.

To ensure the quality of the automatic pipeline, we compared the results to the standard manually derived microstates. In a preliminary analysis, 20 out of the 288 total datasets were used: 10 HC and 10 MA. Figure 4 shows example power spectra in channel POz from one subject after undergoing preprocessing with both the automatic and the manual pipeline, respectively. Specifically, within the lower frequency band, the automatic pipeline acted more conservative in removing noise. This can be attributed to the inability of the automatic pipeline to remove independent components related to motion artifacts. There seems to be significant noise retained from the automatic pipeline causing the alpha peak to shift to a lower frequency,

obstructing our ability to identify the correct frequency. In contrast, there seems to be a significant noise reduction within the delta (1-4Hz) and theta band (4-7Hz) when using the manual pipeline. However, analyzing on a subject level can often introduce noise that is relevant per subject (e.g. subject movement artifacts or individual differences within neural paths). Group level analysis can reduce the noise by averaging out the signals and enhancing neural signals common amongst all subjects (see Figure 4). In the manual pipeline, the noise within the theta band was significantly reduced to obtain the highest optimal neural signal evinced by the alpha peak. Due to limitations of the automatic pipeline, the calculated alpha peak became slightly lower than the manual calculation.

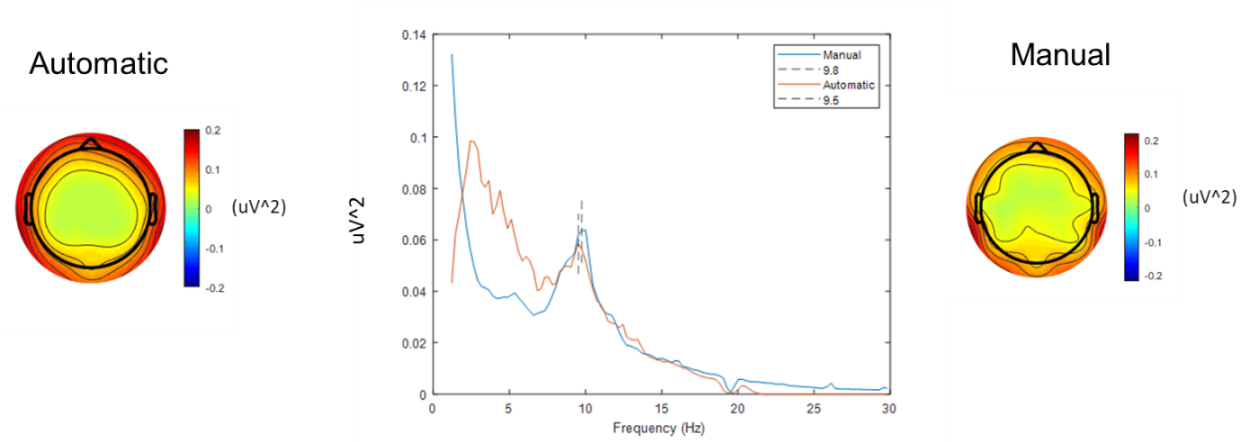

Figure 5: Grand average of preprocessing outcome by automatic (left) and manual (right) pipelines, in a subset of randomly selected 20 subjects.

The spectrum was calculated from the signal at POz electrode and the topography shows the amplitude of EEG at the peak in the alpha band, illustrated by a dashed line on the spectrum.

There are three possibilities that could have induced such a shift in the automatic pipeline: 1) different ways of removing motion artifacts 2) different parameters used for filtering 3) different ways in removing ICs. First, motion artifacts that were elucidated after ICA were not

removed in the automatic pipeline. However even after removing much of the motion artifacts censored by the fMRI time course, on average 95% of the data remained and yet not much of a significant noise reduction was found. Second, the high cutoff band started from 1Hz in the automatic pipeline and 0.5Hz in the manual pipeline; these parameters were set based on previous literature with 1Hz from Wong et al. (2018) and the most frequently used, 0.5Hz. Third, artifacts evinced by ICA (e.g. blink, cardiogram, MR noise) were not properly removed from the automatic pipeline yet were manually inspected and removed in the manual pipeline.

Although after group analysis, a comparable SNR of our analysis was reached, more evidence to support the commonality between manual and automatic pipelines was still needed.

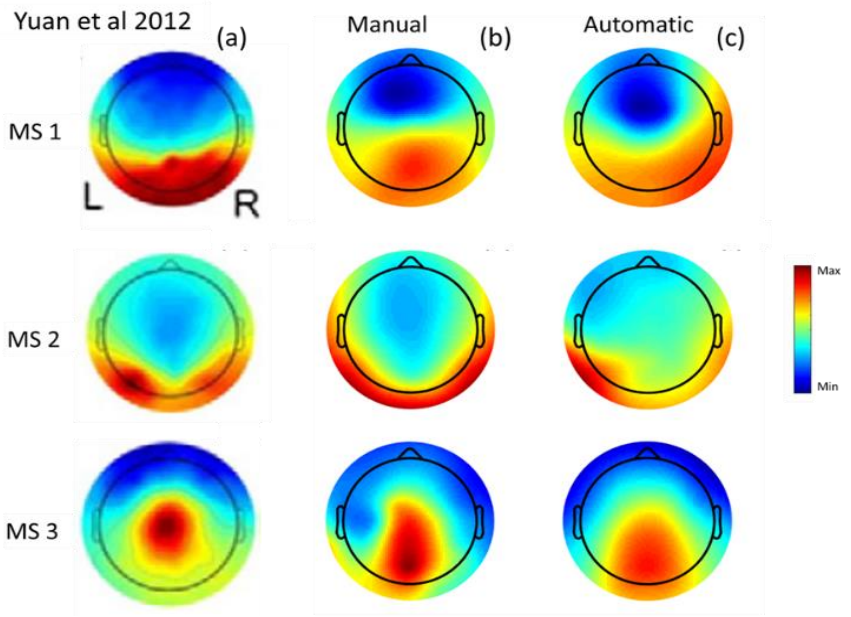

Figure 6: Pipelines produced MS show spatial similarities with Yuan et al. (2012). Three pairs of the most significant spatial correlations related to neural activity between manual (b) and automatic (c) pipeline compared with microstates adapted from Yuan et al. 2012.

The next step after preprocessing was microstates (MS) analysis. Processing the data using MS as described by Yuan et al. (2012) improved the SNR. It did so by extracting the global field power, then underwent another round of independent component analysis, and extracting the maximum MS at each timepoint. Figure 5 shows the MS that were derived from the preliminary data.

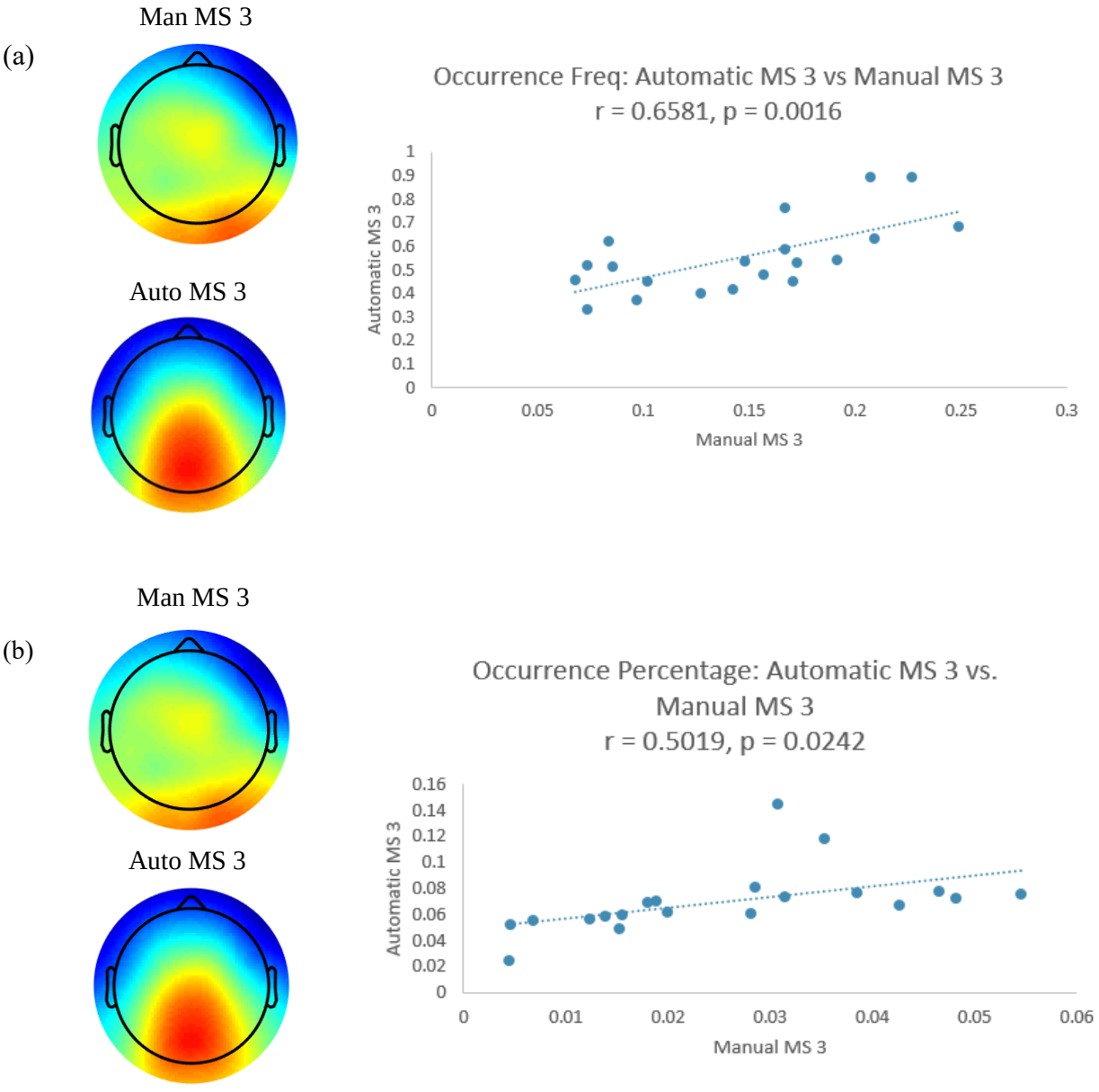

Figure 7: Two temporal dynamic metrics from each pipeline show significant similarities.

The occurrence frequency (a) and percentage (b) from one representative MS, i.e. MS 3, are compared and correlated to measure similarity between both pipelines; Pearson's coefficient proved to be significant with a $p<0.01$ and $p<0.05$, respectively.

The two most spatially similar microstates relevant to neural activities were significantly correlated by using a bootstrapping permutation test. Importantly, we were able to replicate some of the relevant microstate seen in previous literature (Yuan et al 2012). With high spatial correlations across both pipelines, temporal dynamics were then correlated to confirm that pipeline was acceptable. The MS improved the SNR to a commensurable amount thus allowing us to see the significant correlation. In Figure 5, we identified three pairs of microstates from each pipeline that have the highest spatial similarities with Yuan et al. 2012. Albeit these microstates had high spatial correlation, their temporal correlation did not necessarily follow, due to limitations of our algorithm. In fact, looking at a possible salience network, MS 3, the two highest correlated spatial topographies did not produce a significant correlation within their temporal dynamics. In figure 7, we see that another relatively high spatial correlation yielded a high temporal correlation in MS 3. With a significant correlation between the automatic and manual pipelines, we decided to move forward with the automatic pipeline for the big data analysis.

3.2: Associating EEG-ms with fMRI default mode network

3.2.1: Spatial matching of EEG-ms-informed network with DMN template

The current analysis removes discrepancies with participants with comorbidities with other disorders, 232 MA and 56 HC subjects were left for analysis. Figure 7(a) shows all the

relevant microstate topographies from HC and Figure 7(b) shows MA that were derived after group-level ICA. Each independent component (IC) will become a microstate. Each of these microstates has an independent time course and these independent time courses were used as regressors for the GLM. The GLM produced statistical maps of those regions of the brain that were significantly correlated to the EEG regressors.

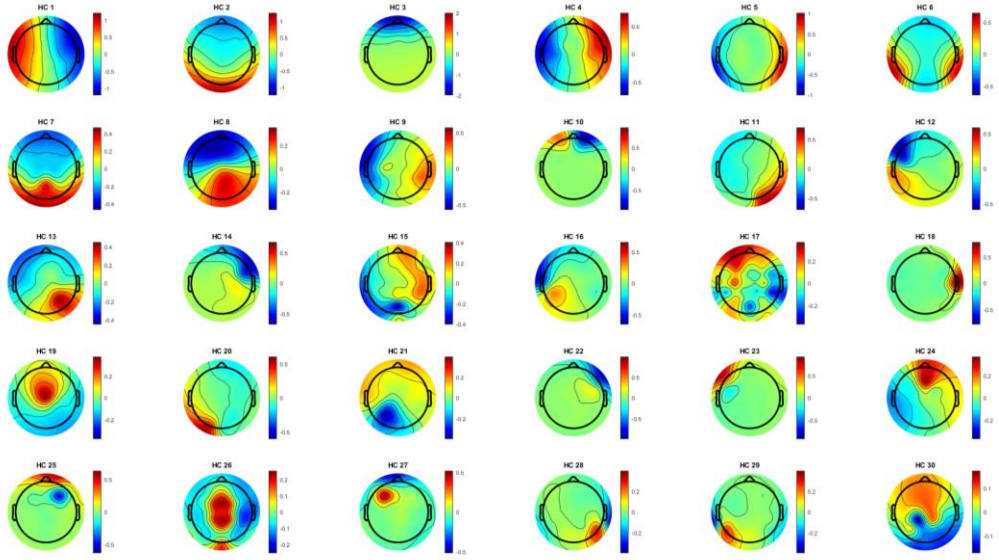

(a)

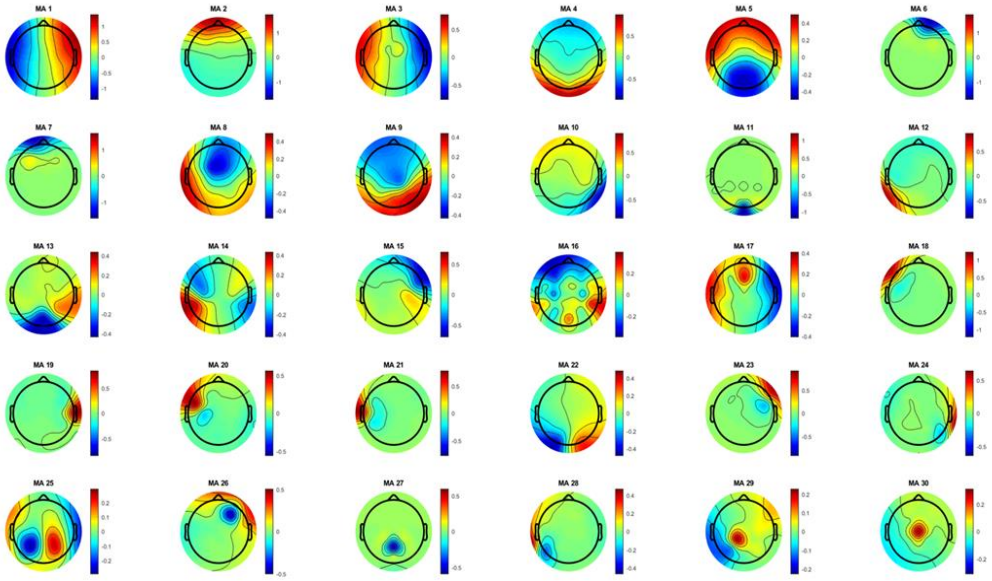

(b)

Figure 8: Topographies of all EEG-ms.

Healthy Control (HC) topography (a) and group level analysis with 30 relevant ICs and Mood Anxiety (MA) topographies from group level ICA. Each topographical map was an independent component of EEG signal. Each component became an EEG microstate and the time course of each microstate became the regressor in the GLM analysis to create statistical maps shown in figures below. Notable microstates include HC 7, HC 19, MA 8 and MA 9.

Of the 30 ICs derived from each group level ICA, four MS were found. These four were visually inspected to have the highest spatial correlations with Yuan and colleagues (2012). With MS 1,7 and 8 representing the default mode network with most of the activity are localized in the posterior regions of brain and MS 10 representing the anterior salience network, with high

activations near the frontoparietal regions. These microstates were chosen by visual inspection of the EEG-ms topography most similar to Yuan et al. 2012.

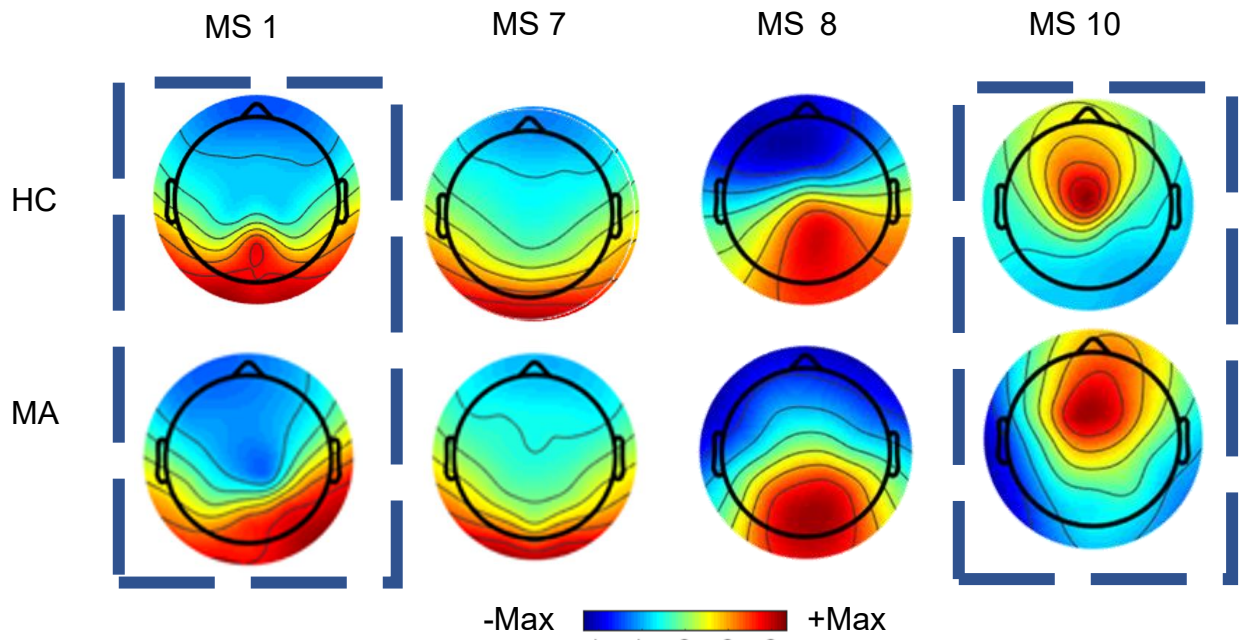

Figure 9: Microstates are identified in HC and MA groups.

The pairs of microstates in dashed lines show distinct features between MA and HC groups.

Namely, two important networks were of importance due to their prevalence in the MA research. Previous studies have shown connections between dDMN and depression and aSN with anxiety disorders (Yuan et al., 2018). Thus, these two types of MS are most critical to studying MA.

(a) dDMN Stanford Template

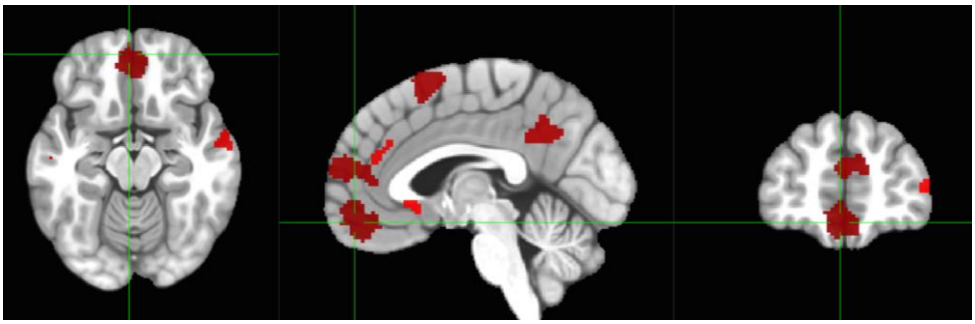

(b) Thresholded group MA IC 9 GLM

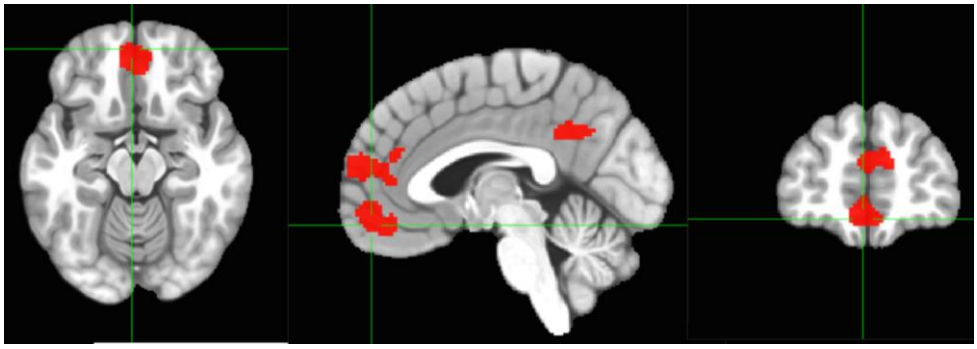

(c) MA IC 9 Overlapping regions between template and thresholded GLM (Dice Coefficient = 0.21)

Figure 10: dDMN-associated network in group-level MA.

In the MA cohort, MS1-informed fMRI analysis showing the relevant brain activations that are most likely produced by the default mode network. (a) Dorsal default mode network template used for spatial comparison. (b) Thresholded GLM ($p_{corrected} < 0.05$) that shows the regions of the brain that significantly correlated with EEG-ms (specifically HC IC 7) time course. (c) To

visualize the dice coefficient between the template and the thresholded GLM to significance, we showed the overlapping regions of GLM.

To show that EEG-ms can elucidate networks that can also be seen in fMRI, we investigated the default mode network. As seen in previous studies, the DMN has distinctive characteristic in EEG topographic data with most of the brain activity concentrated in the posterior region of the brain (Yuan et al., 2012).

In Figure 10, the dorsal default mode network (dDMN) is seen in the template (Figure 10a). The areas that are most activated are the medial prefrontal cortex (MPFC) and the posterior cingulate cortex (PCC) (Shirer et al., 2012). In our GLM results after thresholding (see Figure 10b), we also saw regions of the MPFC and PCC regions significantly correlated with the EEG regressor. This means that our EEG-ms MS 9, was very similar to a DMN topography. The significance of the similarity was determined by the dice coefficient. To visualize how large the dice coefficient was, Figure 10c shows the overlapping regions between the thresholded GLM and the template. The dice coefficient was calculated to be 0.21. This was the highest dice coefficient seen in the MA cohort with respect to the DMN.

3.2.2: Statistical significance of dice coefficient between template to thresholded MS-informed network in MA

While functional MRI was able to pinpoint the anatomical regions of the DMN, simultaneous EEG offers fast temporal dynamics that facilitate relating them to the severity of symptoms. Regarding dorsal DMN, the comparison between the fMRI MA RSN found in our data and the template RSN is shown in Figure 10. We can see the difference between IC 9

compared to other ICs with respect to dice coefficient for the default mode network template shows that IC 9 is significantly correlated.

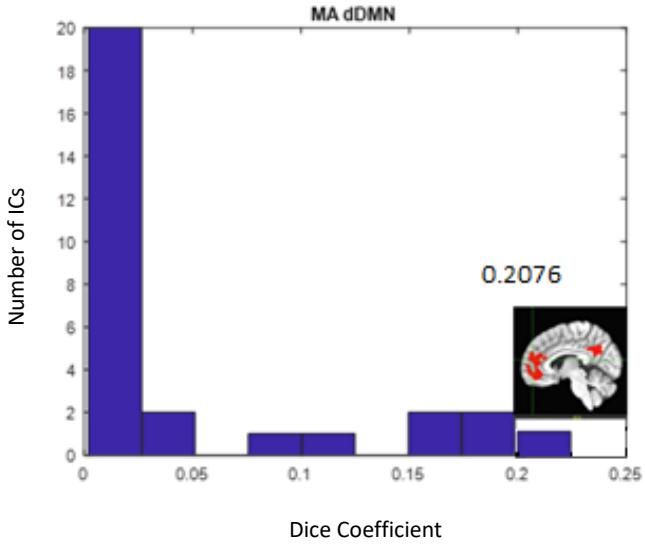

Figure 11: MS 1 in the MA group has the largest dice coefficient with DMN template. Distribution of all MA spatial dice coefficients compared with 29 other ICs with respect to DMN template. The image shows the overlapping regions of IC 9 and is above its corresponding dice coefficient (0.21).

To see how significant the dice coefficient was, we performed a random permutations test. See Figure 11 to see how IC 9 placed in respect to a randomization of over 20,000 other possible dice correlations. It is evident that our findings for this correlation is significant because it lies farther outside the 95% confidence interval of the histogram. This means that we have found an EEG-ms that represents the dDMN.

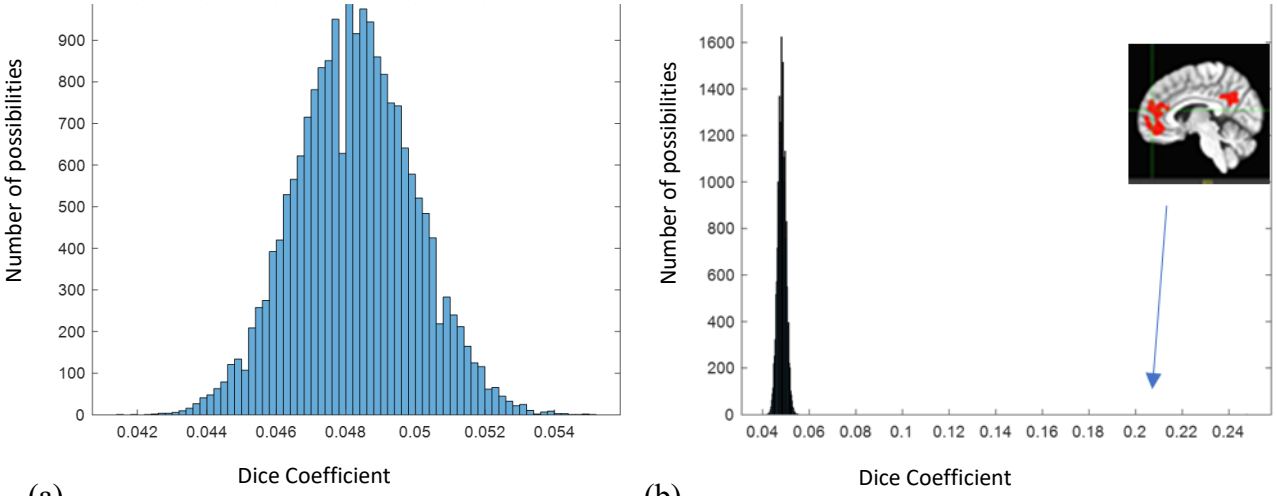

Figure 12: MS 1 of the MA group is the dDMN-associated MS network.

(a) 20,000 random permutations histogram of possible dice coefficient between DMN template mask and thresholded GLM (b) including the dice coefficient of IC 9 MS-informed network thresholded. In both (a) and (b), the x domain is the possible dice coefficients that can be created from the binary mask of the template and the thresholded GLM. The y-axis is the total number of times the dice coefficient was permutated. The arrow pointing down from the image of IC 9 shows its relative location of its dice coefficient on the x axis compared to 20,000 other possible permutations of finding a dice coefficient.

This dDMN-associated microstate had the strongest association to the template among all other microstates and templates.

(a) dDMN Stanford

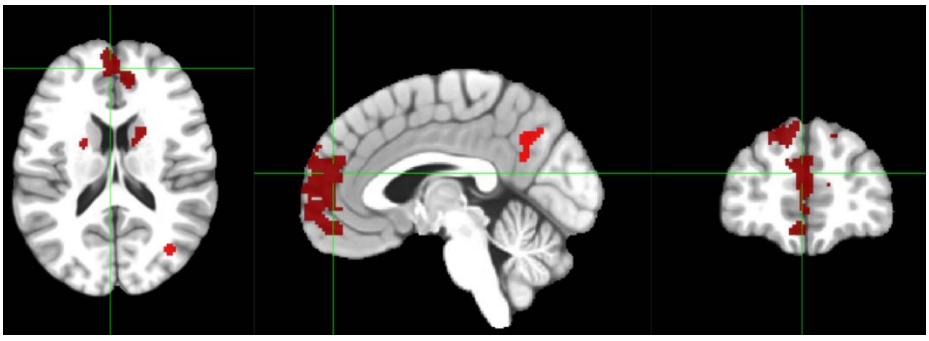

(b) Thresholded group HC IC 7 GLM

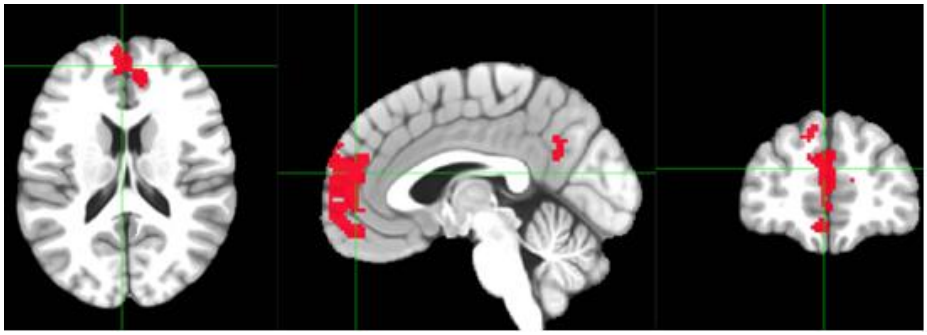

(c) HC IC 7 Overlapping regions between template and thresholded GLM (Dice Coefficient = 0.17)

Figure 13: MS1-informed network in group-level HC.

MS-informed network in group level HC with the crosshair located on the regions of the brain that are significant to the DMN. (a) dorsal default mode network template used for spatial comparison. (b) Thresholded GLM ($p_{corrected} < 0.05$) that shows the regions of the brain that significantly correlated with EEG-ms (specifically HC IC 7) time course. (c) To visualize the dice coefficient between the template and the thresholded GLM to significance, we showed the overlapping regions of GLM.

Once again, we were able to see a significant correlation with the dDMN in the healthy group. In figure 13, we can visually see the overlapping regions of the GLM to the template. To confirm our inspection, we performed the following statistically analysis.

3.2.3: Statistical significance of dice coefficient between template to thresholded MS-informed network in HC

In Figure 13, IC 7 MS-informed network has a significantly higher spatial dice coefficient (Dice Coefficient = 0.17) compared to other ICs.

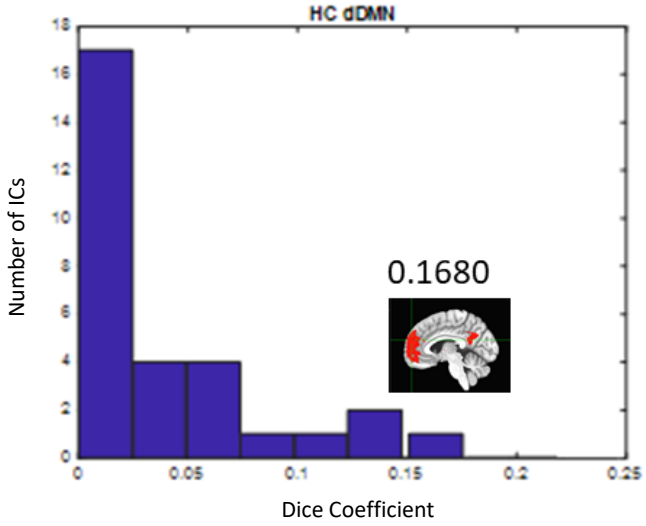

Figure 14: HC IC 7 shows the highest similarity with dDMN template.

Distribution of HC spatial dice coefficients of all 30ICs with respect to DMN template, with the highest correlated dice coefficient shown by the fMRI image of statistically significant correlation with IC 7. The histogram shows where IC 7 compares to other ICs.

Statistically speaking it is very likely that this is a significant finding considering the random permutations distribution as seen in Figure 14.

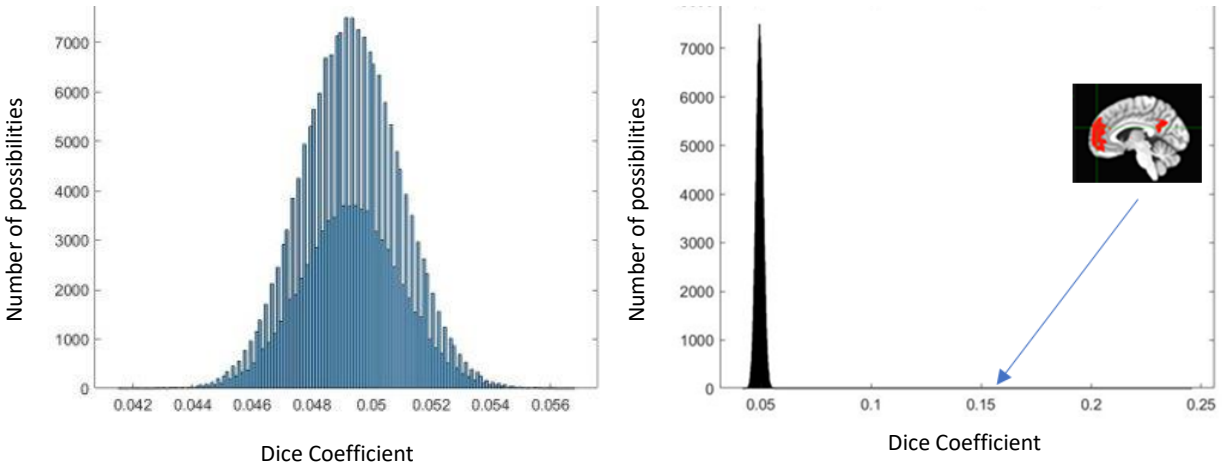

(a) (b)

Figure 15: IC 7 of the HC group is dDMN-associated MS.

(a) Permutations test with all possible voxel permutations for dice coefficient between DMN template mask and thresholded GLM for HC IC 7 (b) including the dice coefficient of IC 7 MS-informed network thresholded. In both (a) and (b), the x domain is the possible dice coefficients that can be created from the binary mask of the template and the thresholded GLM. The y-axis is the total number of times the dice coefficient was permutated. The arrow pointing down from the image of IC 9 shows its relative location of its dice coefficient on the x axis compared to 20,000 other possible permutations of finding a dice coefficient.

Here, we selected the fMRI RSN from our data and compared it to the dDMN RSN template from Shirer et al. (2012) in both MA and HC cohorts. The fMRI RSN and their corresponding EEG-ms-informed network were designated with the same label of best-matched template RSN.

3.2.4: Associating EEG-ms occurrence frequencies with clinical scores

MA Group

Now that we have elucidated that our EEG is indeed associated with fMRI network for DMN, we expected that our EEG-ms could replicate and mirror results as seen in clinical tests. We can look at the how often does the microstate appear during the duration of the recording. This allows us to quantify and characterize how networks can change dynamically. Here we compared the Ruminating Response Score (RRS) with EEG-ms IC 9 in MA. See Figures 23-25 for more details.

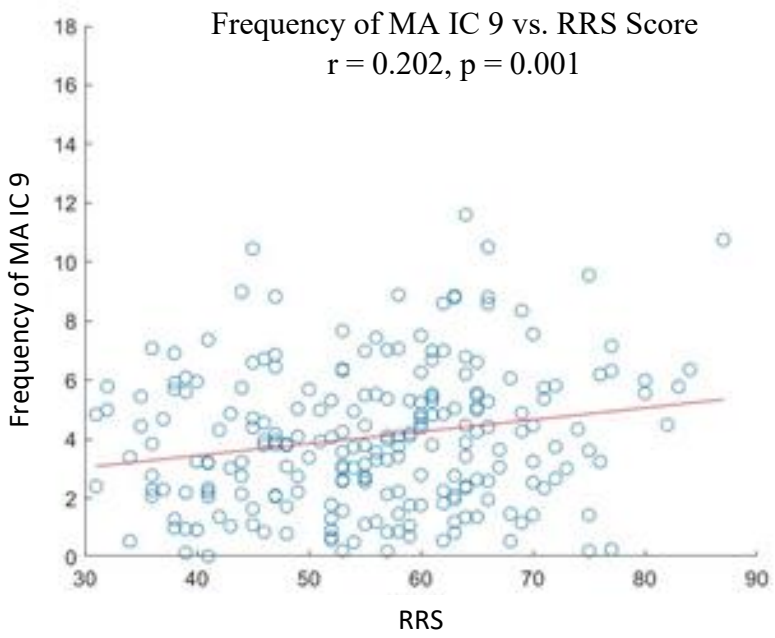

Figure 16: Rumination can affect the occurrence frequency of dDMN-associated MS.

To quantify one's rumination, 21-question RRS was used for all MA participants, matched with each participant's occurrence frequency of IC 9. The Pearson correlation determined the strength of the relationship (r = 0.20, p = 0.001).

Figure 16 shows a significant correlation (corrected for Bonferroni, $p = 0.031$) between the frequency of MA IC 9 and the overall ruminating response score. This strong positive correlation shows that as one begins to show higher degrees of ruminative symptoms, or more MA symptoms, the occurrence rate of the default mode network increases.

Within the RRS, the RRS-reflective sub-score also had a significant positive correlation with a p-value after Bonferroni correction of 0.003. Reflection is a positive coping mechanism that can help one adapt to similar situations and has been shown to predict lower levels of depressive symptoms. Interestingly, others have seen depression correlate higher with DMN dominance with respect to maladaptive rumination (e.g. brooding) as compared to adaptive rumination (e.g. reflective) (Hamilton et al., 2015).

HC Group

Looking at the frequencies of IC 7 in the HC group, we first examined the normality of the distribution of occurrence frequency scores. After passing the Shapiro Wilks test, we then moved forward with our analysis. We saw a strong, positive linear relationship between the occurrence frequency of the EEG-ms and the RRS-D sub score. However, this relationship was not significantly strong enough to hold. No significant temporal correlations were produced within the HC cohort. This is probably due to the flooring effect, where typically healthy subjects score lower, without any significant correlations, on psychological exams.

Importantly, the occurrence rate of dDMN-associated EEG microstates shows distinctive temporal dynamics between the HC and MA groups (i.e. higher in the MA group).

3.2.5: Comparing HC and MA dDMN-associated networks

After confirming the dDMN-associated networks from each cohort, we performed temporal analysis looking specifically at occurrence frequency of each MS-1 network. We found a stark contrast between the HC and MA, supporting our hypothesis that using MS is robust enough to differentiate between the groups.

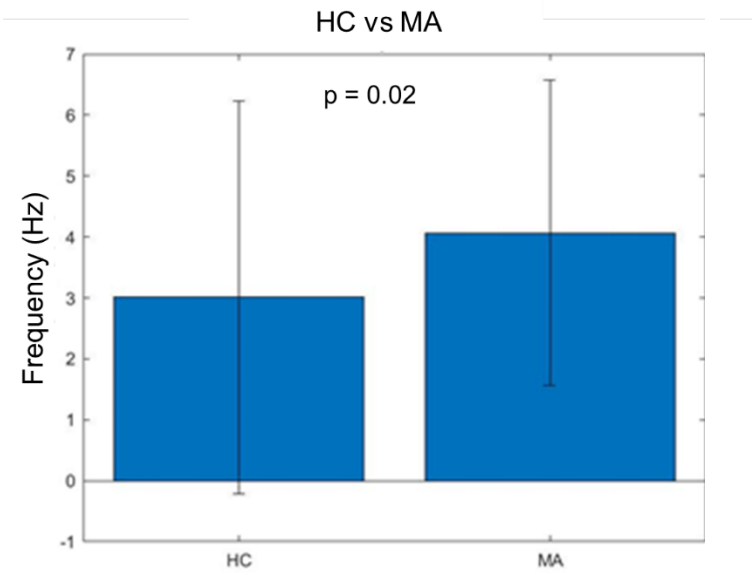

Figure 17: Greater occurrence frequency of DMN-associated networks in MA than HC. T test shows significance (p = 0.02) between the HC and MA cohorts in DMN related EEG-ms. The y-axis shows the occurrence frequency (Hz) of the EEG-ms associated with dDMN. The standard deviation is also denoted.

The difference within the occurrence rate of HC IC 7 and MA IC 9 between HC and MA groups was significant (p = 0.02). Now that we can see the difference between the two groups, this elicits the possibility if there is a progression of one's symptoms to their MS temporal dynamics. Thus, Pearson correlation was calculated over the different clinical and psychological

tests, while correcting for Bonferroni ($p < 0.05$), and found that the RRS displayed high correlation with the dDMN-associated MS occurrence frequency.

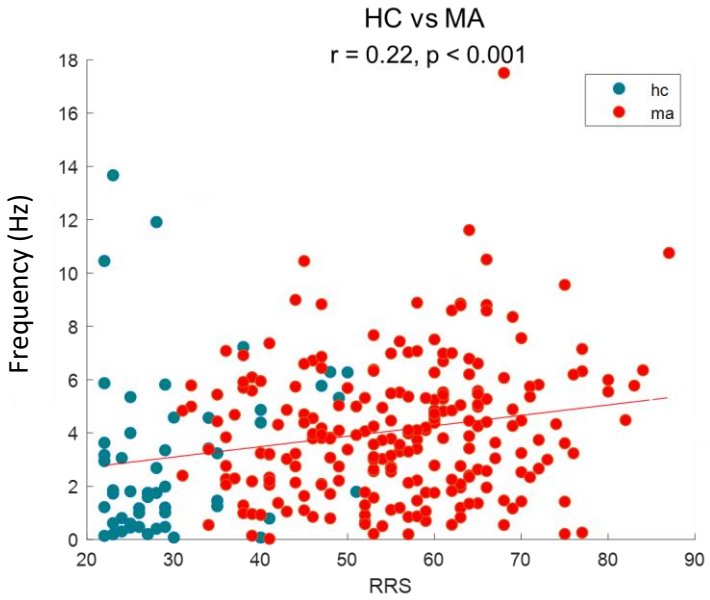

Figure 18: Occurrence frequency of dDMNs compared to RRS scores in both MA and HC. The plot shows a strong linear relationship between the RRS scores and the occurrence frequency of DMN-associated MS ($r = 0.22$, $p < 0.001$).

Evidently, there is a strong correlation within the MA group as seen in Figures 16 and 18. This means that as one progresses into greater ruminative behavior, their EEG-ms can reflect these changes. However, when combined with the healthy cohort, it is further revealed that the correlation extends across the groups. The HC cohort can be easily distinguished. We can conclude that as the frequency of the dDMN-related MS becomes more prominent, it can be an indicator of depressive tendencies.

3.3: Associating EEG-ms with fMRI anterior salience network

3.3.1: Spatial matching of EEG-ms-informed network with SN template

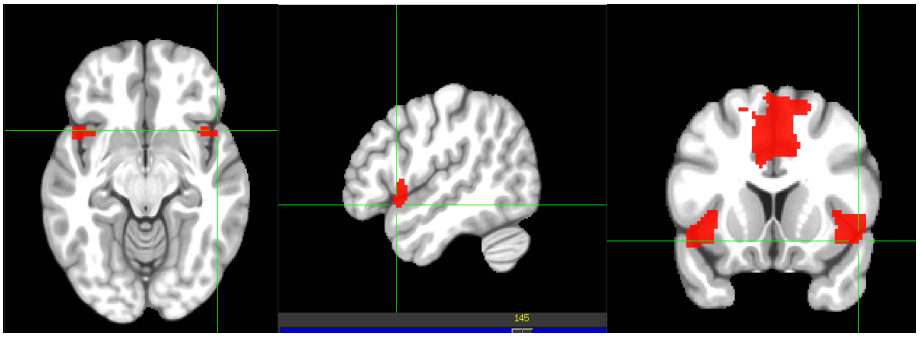

(a) aSN Stanford Template

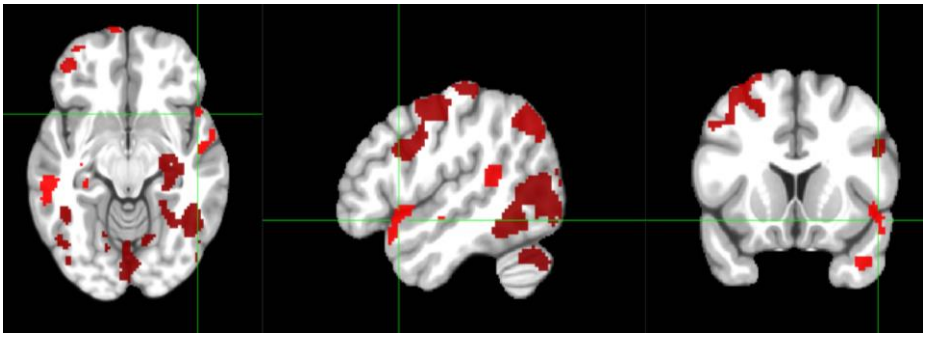

(b) Thresholded group MA IC 8 GLM

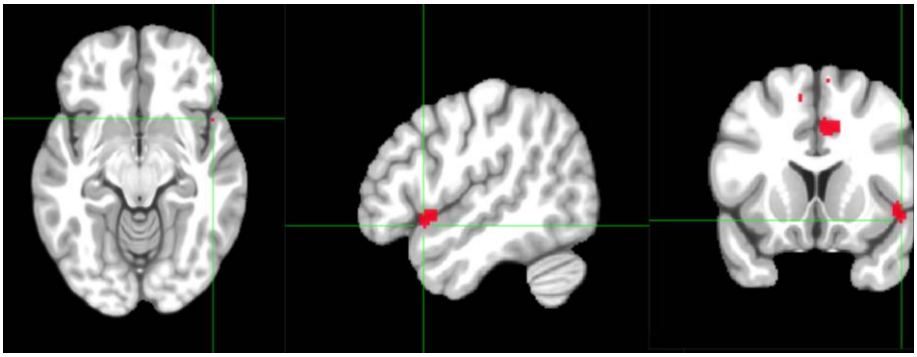

(c) MA IC 8 Overlapping regions between template and thresholded GLM (Dice Coefficient = 0.04)

Figure 19: aSN-associated network in group-level MA.

The crosshairs are located on the regions of the brain that are significant to the DMN. (a) Dorsal default mode network template used for spatial comparison. (b) Thresholded GLM ($p_{corrected} <$ 0.05) that shows the regions of the brain that significantly correlated with EEG-ms (specifically

HC IC 7) time course. (c) To visualize the dice coefficient between the template and the thresholded GLM to significance, we showed the overlapping regions of GLM.

Here, we show the MA cohort's ms-informed RSN associated with the anterior salience network (aSN). Regions that are anchored in the aSN include anterior insular and dorsal anterior cingulate cortex (Toga, 2015). However, after correcting our p-value, we were only able to see surviving activations in the anterior cingulate cortex (ACC).

3.3.2: Statistical significance of dice coefficient between template to thresholded MS-informed network

As outcomes of the matching procedure, i.e. IC 8, became the salience-associated microstate upon EEG topography inspection. However, the highest dice coefficient between an EEG-ms to aSN template was not the IC 8, in fact the highest dice coefficients were of noisy ICs.

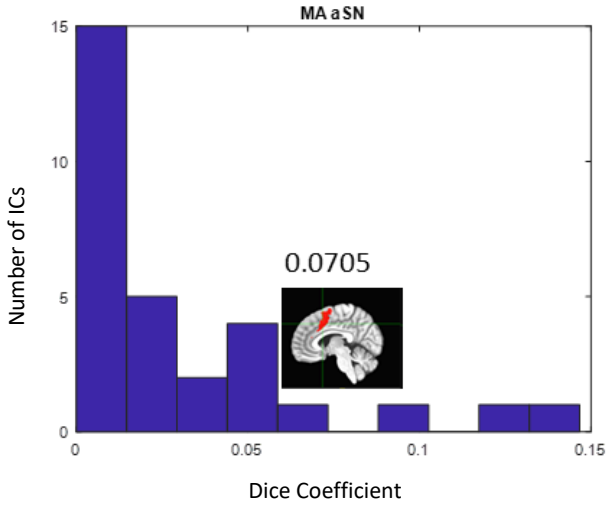

Figure 20: Histogram of all dice coefficients with aSN template and MA microstates. The image above shows the dice coefficient of IC 8 that had the best matched EEG topography map.

The permutations test also further strengthened that this was a plausible EEG-ms-informed network after performing 20,000 iterations of possible dice coefficients from the masked thresholded GLM results. No significant correlations were gleaned from HC cohort in aSN.

Chapter 4: Discussions

In this study we investigated and compared the electrophysiological signatures of RSNs from cohorts of MA and HC individuals. We found four RSN microstates that concurs with previously reported EEG-ms topographies (Yuan et al. 2012, Yuan et al. 2018).

4.1: Quality check between automatic pipeline and manual pipeline

In 3.1 we showed the veracity of the automatic pipeline for the preprocessing of our big data. Although we did not see strong noise removal capabilities on subject level, we were able to improve the signal to noise ratio on a group level. These results proved acceptable to continue.

Nonetheless, compared with the manual pipeline, the automatic pipeline showed higher activities in the lower frequency range (delta and theta band), which correspond to the cardioballistic artifacts. In manual preprocessing, the cardioballistic artifacts were removed in two steps, including average artifact subtraction and the independent component analysis. The quality check and comparison suggest that the automatic pipeline could be further improved by integrating a rejection of independent component analysis to remove the artifacts.

4.2: Associating EEG-ms with fMRI default mode network

In 3.2, we were able to classify one important network prominent in MA group: the default mode network (DMN). Previous studies have shown the significance of DMN in regard to those with mental disorders, and even more widely studied: depression. Here, we were able to replicate similar results. We found the DMN in the EEG topography and correlated it with the

fMRI data. The strength in the spatial correlation in fMRI with the Stanford template shows that our findings were significant.

Spatially, we were able to support our hypothesis in that the dynamic EEG-ms was able to reflect fMRI networks. More specifically our findings show that the dDMN was the most prominent network identified. It had the highest matched dice coefficient in both groups. In MA, DMN regions of the brain specifically the ventromedial prefrontal cortex, remained significant even after multiple corrections tests. This shows that this region of the brain is indeed activated on a group level analysis throughout most MA patients. However, in the HC group, very small regions of the DMN survived after multiple comparisons test. Evidently, the dDMN is more prominent in the MA group than HC.

Temporally, we found significance in the occurrence rating of our DMN-related MS, IC 9. Specifically, with occurrence frequency, or frequency regarding the dominance of the specific RSN, in this case DMN, we saw that it had significant correlations with the depression psychological scores specifically within RRS. This means that as one begins to ruminate more, the more frequent the DMN-related EEG-ms began to appear to dominate the brain. The greater the occurrence rate for our DMN-related EEG-ms suggests a stronger presence against other RSNs. Our findings corroborate with previous studies in the relationship between rumination and depression. Higher levels of rumination are predictors of more severe depressive symptoms in depressed patients and a predictor of depressive symptomatology in non-depressed individuals. Although ruminative responding is not considered a criterion of depression in either DSM-5 or ICD-10, measures of ruminations are nonetheless consistently able to differentiate depressed from never-depressed individuals. Thus, many have posited that rumination is a central aspect of

phenomenology of MDD. Meta-analyses have shown that patients with major depression have increased connectivity within regions of the DMN (Hamilton et al., 2015).

However, when looking into the sub-score of RRS, the reflective sub-score had a significant impact on the general rumination score. This reflective score shows that these patients were able to positively cope and adapt to certain situations. This appears to counter previous findings that higher DMN dominance was associated with higher levels of maladaptive rumination about depressive symptoms and with lower levels of more adaptive reflective rumination (Hamilton et al., 2015). Nonetheless, our findings confirmed the relevance of rumination with DMN in the depression. And more importantly, showed that the rumination-DMN association exist across the diagnostic groups, in depression, anxiety and those comorbid depression-anxiety.

Our findings suggestion that the DMN might be a target of intervention in the heterogeneous MA disorders. Through modification of rumination behavior, the abnormal neural circuit may be modified (Hamilton et al., 2015). However, in the HC we were not able to see any significant findings between the occurrence ratings and clinical scores. We speculate that flooring effect may be the culprit.

We also saw that EEG-ms occurrence frequency is sensitive enough to detect the differences between MA and HC by comparing the EEG-ms between the two groups. As seen in Figure 17 we saw that the occurrence frequency between the MA and HC was significant. This is a promising result and furthers the findings of previous literature in that dDMN is more common and more prevalent in those with MA (Mulders et al., 2015). Albeit, more improvements like noise removal may be needed to distinguish their differences more powerfully.

All in all, we can see that EEG-ms is a feasible alternative for characterizing MA specifically in characterizing depression symptoms.

4.3: Associating EEG-ms with fMRI anterior salience network

Unfortunately, no EEG-ms relating to aSN were found nor were there any related correlations with clinical scores. The aSN consist of key limbic and prefrontal regions that are engaged in development of anxiety, such as amygdala, anterior insula, and dorsal anterior cingulate cortex. Studies have shown that there is a link between higher trait anxiety that may underlie altered salience processing and cognitive regulation (Geng et al., 2016), thus we expected to see changes within anxiety clinical and psychological scores relating to the dynamics of the salience network.

Neither MA nor HC group within the anterior salience network yielded significant spatial dice coefficient. However, in MA, the dice coefficient that was matched was significant after performing random permutations. Only the MA showed that the dACC survived the multiple-corrections test. This may imply that our aSN related EEG-ms had too much noise to indicate more relevant regions with strong correlations in fMRI RSNs.

Temporally speaking, there was a significant difference in the duration of the aSN. However, our results did not match our expectations: the MA had a significantly longer duration than HC. As previous literature has mentioned, the salience network, specifically aSN, is commonly associated with anxiety disorder. Intuitively, with the limbic and prefrontal regions involved, those with a higher prevalence of aSN may indicate higher interoceptive awareness, compared to negative relationships which can indicate lower interoceptive awareness and a connection with anxiety disorder (Paulus & Stein, 2010).

Because the salience network is hidden deep within the cortical structure, it is difficult to capture the brain regions on a scalp level without removing any motion artifacts in the EEG data. This was one of the largest limitations in our study. Further, because we were unable to correctly identify the aSN in the HC cohort, it might contribute to an unexpected temporal correlation between the HC and MA mean durations.

Our findings revealed that the temporal dynamics of the DMN-associated and aSN-associated EEG-ms are associated with depression and anxiety severity, which suggests that such neuroimaging metrics may be used as MA-related biomarkers. While future investigations on such neuroimaging metrics are warranted to fully characterize their relevance to psychopathology of MA, and to clinically relevant outcome measures, EEG-ms have potentials in facilitating the diagnosis and prognosis of MA. Furthermore, since EEG-ms is related to the level of disease severity, it may be used as an evaluation biomarker in determining the effectiveness of an intervention or treatment. The temporal independent microstates based on stand-alone EEG data may be able to provide more portable and less expensive way for researching novel interventions for MA. Another potential use of EEG-ms is as neurofeedback training for user to alleviate the symptom via learning by biofeedback approach (Yuan et al., 2012, 2018). Since instrumentation for EEG-based neurofeedback is considerably affordable and portable, it opens another avenue of use for the EEG-ms.

Chapter 5: Conclusion

Our study has investigated the dynamics of connectivity in the salience network and the default mode network from simultaneous EEG and fMRI data acquired in 297 participants of T1000 Study. Our results for the first time reported that default mode network and salience network are associated with EEG-ms in patients with mood and anxiety disorders, especially at a large sample of more than 200 subjects. Our current findings also have replicated our previous reports of EEG-ms associated with resting state brain networks in heathy individuals (Yuan et al., 2012) and participants with PTSD (Yuan et al., 2018). More importantly, results of the current study for the time reported that, in a heterogenous cohort of patients with mood and anxiety disorder, the temporal dynamics of the default mode network is correlated with the rumination behavior in patients, which is a factor highly relevant to their current depressive symptom and also a risk factor for recurrent depression. The results indicate that dynamic resting state functional connectivity revealed by EEG-ms analysis is a feasible approach for detecting the severity of depression in MA patients, however more efforts are needed to de-noise the data and improve upon the automatic pipeline. By integrating a large dataset and using a fully data-driven approach, 'Big Data' of multimodal EEG-fMRI neuroimaging has the potential to move towards broader clinical use in large-scale clinical research and allow for advanced insights about brain spatiotemporal dynamics in the healthy and diseased populations.

References

Allen, P. J., Josephs, O., & Turner, R. (2000). A method for removing imaging artifact from continuous EEG recorded during functional MRI. *NeuroImage*. https://doi.org/10.1006/nimg.2000.0599

Allen, P. J., Polizzi, G., Krakow, K., Fish, D. R., & Lemieux, L. (1998). *Identification of EEG Events in the MR Scanner: The Problem of Pulse Artifact and a Method for Its Subtraction*.

Brandeis, D., & Lehmann, D. (1989). Segments of event-related potential map series reveal landscape changes with visual attention and subjective contours. *Electroencephalography and Clinical Neurophysiology*, *73*(6), 507–519. https://doi.org/https://doi.org/10.1016/0013-4694(89)90260-5

Brandeis, D., Lehmann, D., Michel, C. M., & Mingrone, W. (1995). Mapping event-related brain potential microstates to sentence endings. *Brain Topography*, *8*(2), 145–159. https://doi.org/10.1007/BF01199778

Cox, R. W. (1996). AFNI: Software for Analysis and Visualization of Functional Magnetic Resonance Neuroimages. *Computers and Biomedical Research*, *29*(3), 162–173. https://doi.org/https://doi.org/10.1006/cbmr.1996.0014

Elliott, R., Sahakian, B. J., Herrod, J. J., Robbins, T. W., & Paykel, E. S. (1997). Abnormal response to negative feedback in unipolar depression: evidence for a diagnosis specific impairment. *Journal of Neurology, Neurosurgery, and Psychiatry*, *63*(1), 74–82. https://doi.org/10.1136/jnnp.63.1.74

Geng, H., Li, X., Chen, J., Li, X., & Gu, R. (2016). Decreased intra-and inter-salience network functional connectivity is related to trait anxiety in adolescents. *Frontiers in Behavioral*

Neuroscience, *9*, 350.

Glover, G. H., Li, T. Q., & Ress, D. (2000). Image-based method for retrospective correction of physiological motion effects in fMRI: RETROICOR. *Magnetic Resonance in Medicine*, *44*(1), 162–167. https://doi.org/10.1002/1522-2594(200007)44:1<162::aid-mrm23>3.0.co;2-e

Goldberg, D. (2011). The heterogeneity of "major depression." *World Psychiatry*, *10*(3), 226–228. https://doi.org/10.1002/j.2051-5545.2011.tb00061.x

Hamilton, J. P., Farmer, M., Fogelman, P., & Gotlib, I. H. (2015). Depressive Rumination, the Default-Mode Network, and the Dark Matter of Clinical Neuroscience. *Biological Psychiatry*, *78*(4), 224–230. https://doi.org/10.1016/j.biopsych.2015.02.020

Paulus, M. P., & Stein, M. B. (2010). Interoception in anxiety and depression. *Brain Structure & Function*, *214*(5–6), 451–463. https://doi.org/10.1007/s00429-010-0258-9

Shirer, W. R., Ryali, S., Rykhlevskaia, E., Menon, V., & Greicius, M. D. (2012). Decoding subject-driven cognitive states with whole-brain connectivity patterns. *Cerebral Cortex*, *22*(1), 158–165.

Mulders, P. C., van Eijndhoven, P. F., Schene, A. H., Beckmann, C. F., & Tendolkar, I. (2015). Resting-state functional connectivity in major depressive disorder: a review. Neuroscience & Biobehavioral Reviews, 56, 330-344.

Sylvester, C. M., Corbetta, M., Raichle, M. E., Rodebaugh, T. L., Schlaggar, B. L., Sheline, Y. I., … Lenze, E. J. (2012). Functional network dysfunction in anxiety and anxiety disorders. Trends in Neurosciences, 35(9), 527–535. https://doi.org/10.1016/j.tins.2012.04.012

Toga, A. W. (2015). *Brain mapping: An encyclopedic reference*. Academic Press.

Treynor, W., Gonzalez, R., & Nolen-Hoeksema, S. (2003). Rumination reconsidered: A psychometric analysis. *Cognitive Therapy and Research*, *27*(3), 247–259.

https://doi.org/10.1023/A:1023910315561

Victor, T. A., Khalsa, S. S., Simmons, W. K., Feinstein, J. S., Savitz, J., Aupperle, R. L., Yeh, H. W., Bodurka, J., & Paulus, M. P. (2018). Tulsa 1000: A naturalistic study protocol for multilevel assessment and outcome prediction in a large psychiatric sample. *BMJ Open*, *8*(1), 1–16. https://doi.org/10.1136/bmjopen-2017-016620

Watkins, P. C., Vache, K., Verney, S. P., Muller, S., & Mathews, A. (1996). Unconscious mood-congruent memory bias in depression. *Journal of Abnormal Psychology*, *105*(1), 34–41. https://doi.org/10.1037//0021-843x.105.1.34

Wong, C. K., Luo, Q., Zotev, V., Phillips, R., Chan, K. W. C., & Bodurka, J. (2018). Automatic cardiac cycle determination directly from EEG-fMRI data by multi-scale peak detection method. *Journal of Neuroscience Methods*. https://doi.org/10.1016/j.jneumeth.2018.03.017

Wong, C. K., Zotev, V., Misaki, M., Phillips, R., Luo, Q., & Bodurka, J. (2016). Automatic EEG-assisted retrospective motion correction for fMRI (aE-REMCOR). *NeuroImage*. https://doi.org/10.1016/j.neuroimage.2016.01.042

Young, K. D., Zotev, V., Phillips, R., Misaki, M., Yuan, H., Drevets, W. C., & Bodurka, J. (2014). Real-time fMRI neurofeedback training of amygdala activity in patients with major depressive disorder. *PLoS ONE*, *9*(2). https://doi.org/10.1371/journal.pone.0088785

Yuan, H., Phillips, R., Wong, C. K., Zotev, V., Misaki, M., Wurfel, B., Krueger, F., Feldner, M., & Bodurka, J. (2018). Tracking resting state connectivity dynamics in veterans with PTSD. *NeuroImage: Clinical*, *19*(October 2017), 260–270. https://doi.org/10.1016/j.nicl.2018.04.014

Yuan, H., Zotev, V., Phillips, R., Drevets, W. C., & Bodurka, J. (2012). Spatiotemporal dynamics of the brain at rest - Exploring EEG microstates as electrophysiological signatures of BOLD resting state networks. *NeuroImage*, *60*(4), 2062–2072.

https://doi.org/10.1016/j.neuroimage.2012.02.031